Liquid Crystals
Publication details, including instructions for authors and subscription information:
http://www.informaworld.com/smpp/title~content=t713926090

Phase transitions and conformational changes in an antiferroelectric liquid crystal 4-(1-methylheptyloxycarbonyl)phenyl 4'-octyloxybiphenyl-4-carboxylate (MHPOBC)

Kyeong Hyeon Kim[a]; Yoichi Takanishi[a]; Ken Ishikawa[a]; Hideo Takezoe[a]; Atsuo Fukuda[a]
[a] Department of Organic and Polymeric Materials, Tokyo Institute of Technology, Tokyo, Japan

To cite this Article Kim, Kyeong Hyeon , Takanishi, Yoichi , Ishikawa, Ken , Takezoe, Hideo and Fukuda, Atsuo(1994) 'Phase transitions and conformational changes in an antiferroelectric liquid crystal 4-(1-methylheptyloxycarbonyl)phenyl 4'-octyloxybiphenyl-4-carboxylate (MHPOBC)', Liquid Crystals, 16: 2, 185 — 202
To link to this Article: DOI: 10.1080/02678299408029146
URL: http://dx.doi.org/10.1080/02678299408029146

LIQUID CRYSTALS, 1994, VOL. 16, NO. 2, 185–202

Phase transitions and conformational changes in an antiferroelectric liquid crystal 4-(1-methylheptyloxycarbonyl)phenyl 4′-octyloxybiphenyl-4-carboxylate (MHPOBC)

by KYEONG HYEON KIM, YOICHI TAKANISHI, KEN ISHIKAWA, HIDEO TAKEZOE* and ATSUO FUKUDA*

Department of Organic and Polymeric Materials, Tokyo Institute of Technology, O-okayama, Meguro-ku, Tokyo 152, Japan

(*Received 19 March 1993; accepted 30 July 1993*)

The thermodynamic properties and conformational structures in the crystalline and liquid crystalline phases of 4-(1-methylheptyloxycarbonyl)phenyl 4′-octyloxybiphenyl-4-carboxylate (MHPOBC) have been investigated by Raman scattering, X-ray diffraction and differential scanning calorimetry (DSC). MHPOBC can assume two different crystalline states at room temperature depending on crystallization conditions, and heating transforms the metastable crystal to the stable one before melting. In the liquid crystalline phases, Raman scattering spectra have revealed not only the flip–flop twisting vibration of the biphenyl group but also the internal rotation around C–C bonds between the carbonyl groups and the corresponding benzene rings.

1. Introduction

Since the discovery of tristable switching [1] and the subsequent identification of antiferro- and ferri-electric phases in MHPOBC [2, 3], much research has been reported on basic and the application aspects [1, 4]. However there remain several unresolved problems such as the origin of the appearance of the antiferroelectric and ferrielectric phases especially from the standpoint of molecular structure. Although liquid crystal molecules are treated as rigid rods in most theoretical approaches until now, the molecular conformations and the intermolecular interactions are thought to be the key to understanding the origin of the phases and the transitions between them [5, 6].

To investigate the intramolecular and intermolecular interactions we have studied Raman scattering together with X-ray diffraction. Although characteristic conformational differences among liquid crystalline phases have not yet been clarified in this preliminary study, we report here the first set of results concerning the conformational changes at the crystal–crystal and crystal–smectic phase transitions of MHPOBC by means of Raman scattering as well as X-ray diffraction and DSC analysis. We found that two crystal structures are formed depending on the cooling rate. The transition between these two crystalline phases, and the conformational changes at the crystal–smectic phase transition are also discussed.

*Authors for correspondence.

0267–8292/94 $10·00

2. Experimental procedure

The material used was (*R*)-MHPOBC (see figure 1), which has phase sequence, I(148°C) S_A(122°C) $S^*_{C_\alpha}$(120·9°C) S^*_C(119·2°C) $S^*_{C_\gamma}$(118·4°C) $S^*_{C_A}$(66°C) $S^*_{I_A}$(66 ~ 30°C) C, according to DSC measurements on cooling process. Randomly oriented cells were used throughout the present Raman experiment. Raman spectra were obtained using a JASCO NR-1800 system equipped with a triple monochromator. The excitation source was an Ar^+ ion laser operating at 514 nm with a power of 100 mW. A back scattering geometry and a spectral width of 2·5 cm^{-1} were used for all experiments. The sample was introduced between two glass plates with PET spacers of 350 μm thickness and the sample temperature was controlled within 0·1°C. The thermal behaviour was measured using a Rigaku TAS-100 DSC system equipped with a liquid nitrogen bomb as a cooling unit. The layer thickness was measured by a Rigaku RU-200 X-ray diffractometer according to methods reported previously [7].

3. Experimental results

3.1. *Raman scattering*

Figures 2(*a*) and (*b*) show Raman spectra for different phases (*a*) in the high frequency region (1000–1800 cm^{-1}) and (*b*) in the low frequency region (200–1000 cm^{-1}). In order to illustrate the difference between the spectra at two temperatures in the crystalline phases clearly, spectra in the two indicated regions are expanded in the insets of each figure.

The assignments [8–14] of several peaks are listed in table 1. Peaks at 1736 cm^{-1} and 1713 cm^{-1} are assigned to the C=O stretching at k_1 (between biphenyl and phenyl groups) and k_2 (near the chiral group) in figure 1, respectively, by considering resonance and inductive effects [8, 9]; the assignments are confirmed by comparing the IR absorption peaks of MHPOBC with those of MOPBIC

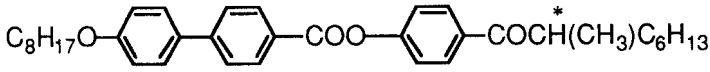

and MHPOCBC

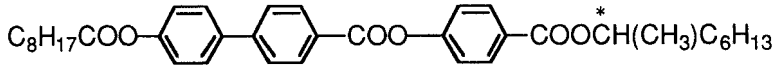

as summarized in table 2.

As shown in figure 2, spectral differences in different phases appear especially for the vibrational peaks which are related to the biphenyl and ester groups. Remarkable changes are observable at around 60–90°C, where the crystal–smectic phase transition takes place. The most conspicuous change is the temperature variation of the Raman peak at around 1190 cm^{-1}, which is assigned to the aromatic C–H in-plane

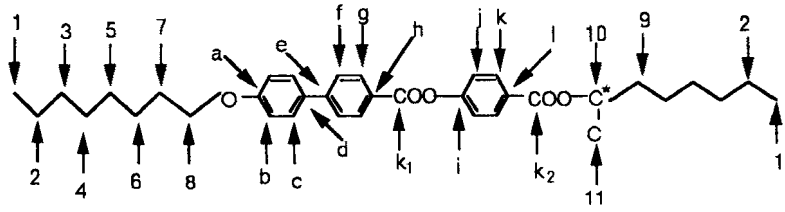

Figure 1. Molecular structure of 4-(1-methylheptyloxycarbonyl)phenyl 4′-octyloxybiphenyl-4-carboxylate (MHPOBC).

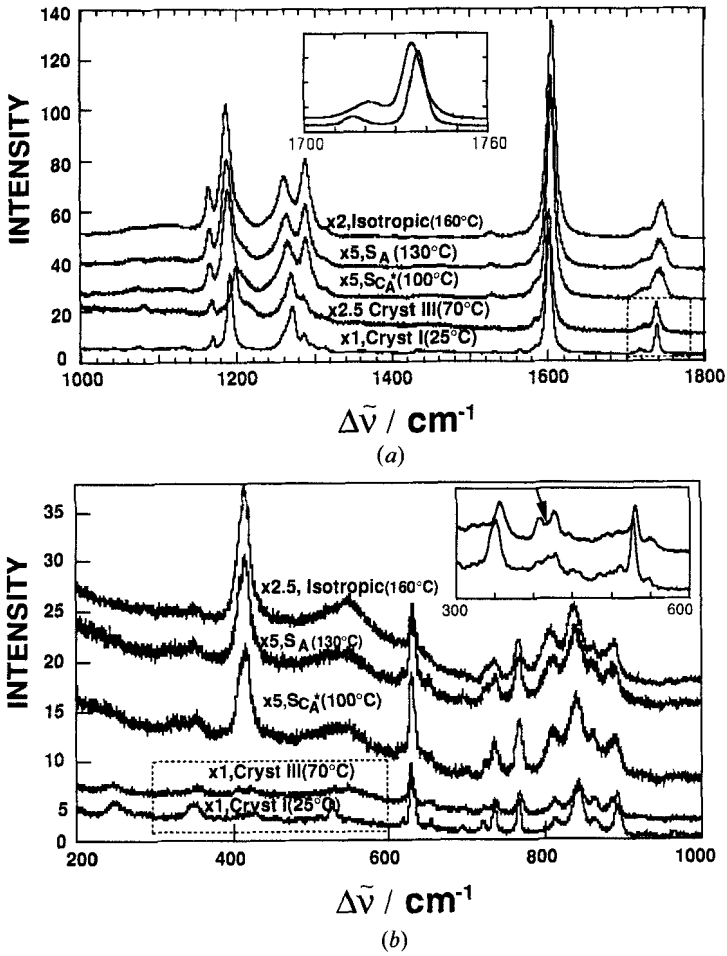

Figure 2. Raman spectra for different phases (*a*) in the high frequency region (1000–1800 cm^{-1}) and (*b*) in the low frequency region (200–1000 cm^{-1}). Insets are to show minute differences in the enclosed areas for two crystalline phases.

Table 1. The assignments of several peaks in the Raman spectra.

$\Delta\tilde{\nu}/cm^{-1}$	Assignment	Reference
1736	C=O stretching at k_1 in figure 1	[8,9]
1713	C=O stretching at k_2 in figure 1	[8,9]
1600	C–C stretching of benzene	[9,10]
1285	C–C stretching in biphenyl link	[11,12]
1270	Asymmetric C–O stretching	[9]
1190	Aromatic C–H in-plane deformation	[10,13]
418	Vibrational mode of twisted biphenyl	[14]

Table 2. The vibrational frequencies of the carbonyl groups in several antiferroelectric liquid crystals.

Structure of mesogens	Positions of carbonyl groups		
	Position 1	Position 2	Position 3
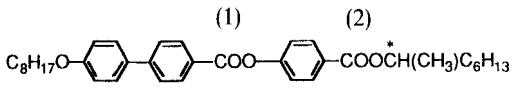	1736·1 cm^{-1}	1713·0 cm^{-1}	—
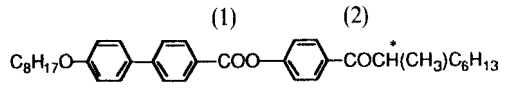	1736·1 cm^{-1}	1680·2 cm^{-1}	—
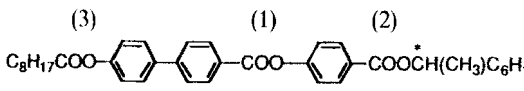	1734·0 cm^{-1}	1720·7 cm^{-1}	1753·5 cm^{-1}

deformation. Figure 3 shows the temperature dependence of this Raman peak. We should notice several characteristics in figure 3: (1) At a slow cooling rate ($-0{\cdot}8°C\,min^{-1}$) the Raman shift gradually increases in the smectic phase, and then shows a discontinuous change at the transition temperature to a crystalline phase ($\sim 66°C$). On the other hand, it monotonically increases at a fast cooling rate ($-3{\cdot}5°C\,min^{-1}$). This suggests the existence of two crystalline phases, depending on the fast and slow cooling rates; these phases are designated as Cryst I and Cryst III, respectively, according to the Hori and Endo's nomenclature [15]. (2) On heating from Cryst I, the Raman shift jumps to 1198 cm^{-1} at 66°C and slightly decreases until the Cryst III–$S^*_{C_A}$ phase transition takes place at about 82°C. At this temperature it discontinuously decreases to the original level, and then decreases again continuously. (3) On heating from Cryst III, the Raman shift gradually decreases with temperature until about 82°C where the Cryst III–$S^*_{C_A}$ phase transition takes place, and then discontinuously decreases to about 1190 cm^{-1} as shown in figure 3 (*b*). Thus, thermal hysteresis is observed in this Raman peak for Cryst III.

The opposite temperature dependence of Raman shift was observed for the peak due to the C=O stretching at k_1 in figure 1. As clearly seen in figure 4 (*a*), the Raman peak jumps by 4 cm^{-1} at the phase transition from Cryst III to $S^*_{C_A}$ and continuously increases with temperature. This change is also associated with thermal hysteresis. It is interesting to notice the contrast observed in the temperature variation of the peak due to the asymmetric C–O stretching, as shown in figure 4 (*b*). This peak decreases as the temperature rises, although the discontinuous change is not so large as compared with that in the C=O stretching. The result implies that the C=O bond stiffening results in the C–O bond weakening at least in the k_1 ester group.

Characteristics of both the C=O bonds are also observed in the temperature dependence of the full width at half maximum; the dependence of k_1 carbonyl is shown in figure 4 (*c*). In contrast to the behaviour of the peak due to the C–C vibration of the phenyl rings (1600 cm^{-1}), which is also shown in figure 4 (*c*), the C=O stretching peak suddenly broadens at the phase transition from Cryst III to $S^*_{C_A}$ and shows thermal hysteresis.

Peak intensities reflect the difference in each phase to some extent. As an example, the relative intensities of 1736, 1600 and 1270 cm^{-1} obtained during a heating process are plotted as a function of temperature in figure 5. The Cryst I–Cryst III transition is

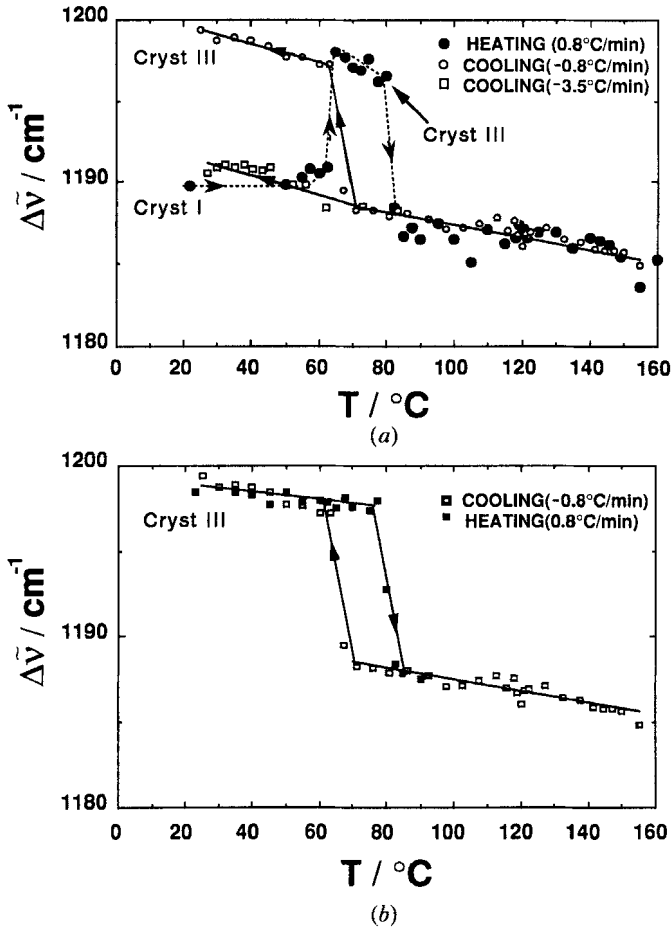

Figure 3. The temperature dependence of the Raman shift for the aromatic C–H in-plane deformation peak obtained by (*a*) cooling at two different rates after heating from Cryst I and by (*b*) cooling after heating from Cryst III.

clearly seen as a large jump in the peak intensity. The Cryst III–$S^*_{C_A}$, S^*_C subphases–S_A, and S_A–Iso transitions are also clearly recognized in the peak intensity variation, although the temperature dependence of the Raman shift is not sufficient to reveal the transition points except for some special cases such as Cryst III–$S^*_{C_A}$. These discontinuities in Raman intensity at the phase transitions may be attributed to either the change of molecular conformation or the orientation of microdomains spontaneously formed in the randomly oriented sample. It is hard, however, to distinguish the changes among the subphases existing between S_A and $S^*_{C_A}$, i.e. $S^*_{C_\alpha}$, S^*_C and $S^*_{C_\gamma}$ due to their narrow temperature ranges.

The most conspicuous intensity changes are observed for the peaks at 418 cm^{-1} and 1285 cm^{-1}, both of which remarkably increase at the Cryst III–$S^*_{C_A}$ phase transition. Figure 6 (*a*) shows the temperature dependence of the relative intensity of the 418 cm^{-1} peak to that of the 1600 cm^{-1} peak. Since the absolute intensities of the spectrum seriously vary with temperature as illustrated in figure 2, the relative intensity is plotted to clarify the 418 cm^{-1} peak intensity variation, based on the reference peak which exhibits the typical temperature dependence. The intensity of the 418 cm^{-1} peak,

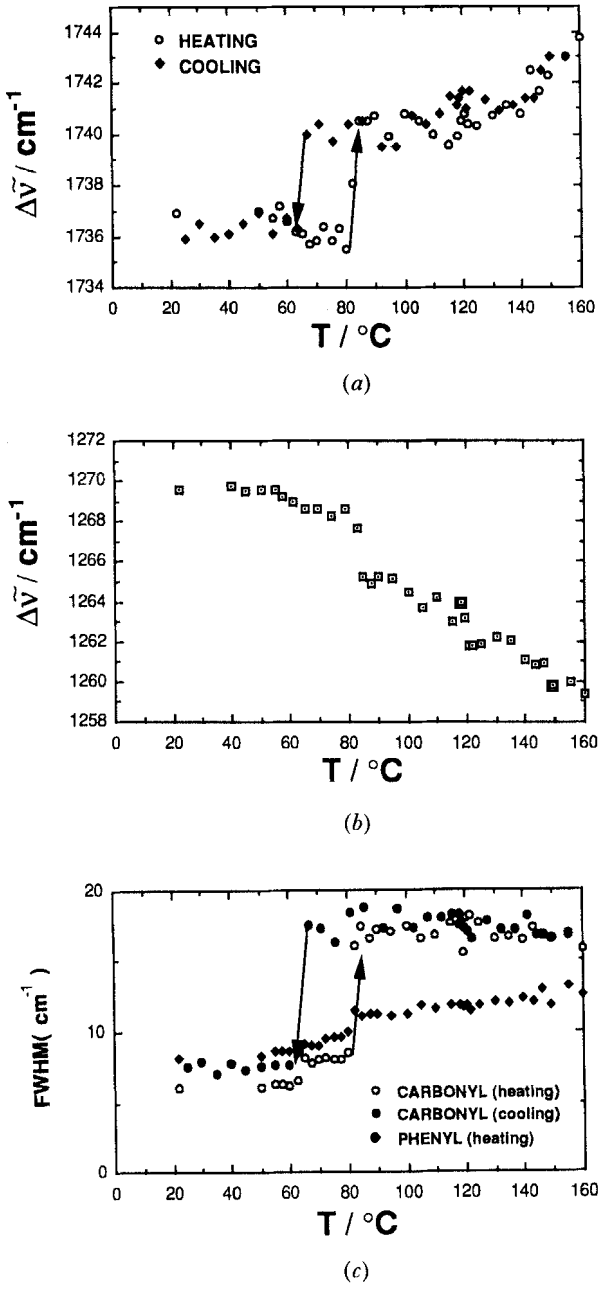

Figure 4. The temperature dependence of (*a*) the Raman shift of the C=O stretching between the biphenyl and phenyl groups, (*b*) the Raman shift of the asymmetric C–O vibration on heating, and (*c*) the full width at half maximum of the C=O stretching peak between the biphenyl and phenyl groups and that of the phenyl C–C stretching (1600 cm^{-1}).

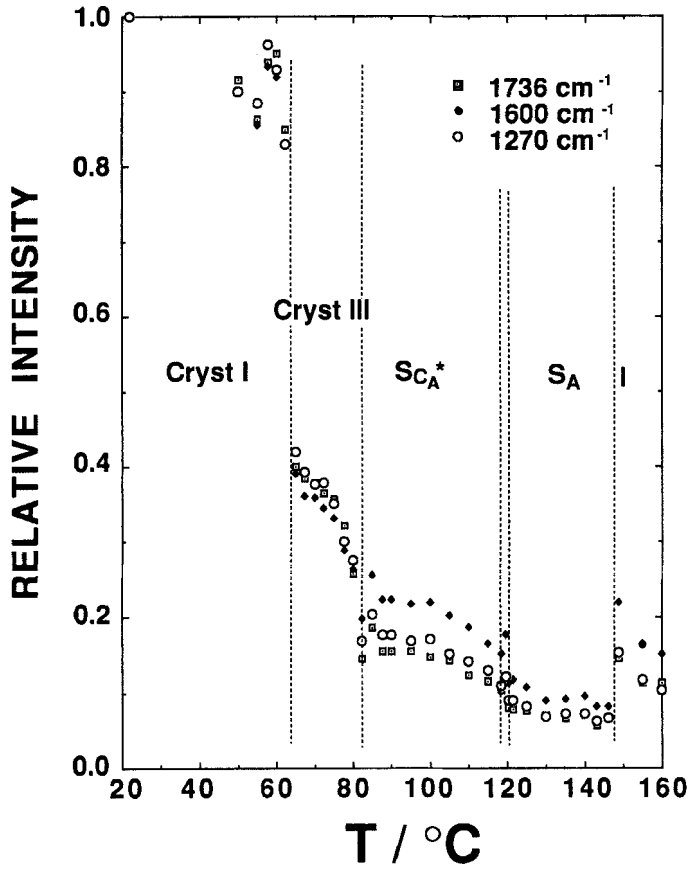

Figure 5. Typical temperature dependence of the normalized intensities of the 1736 cm^{-1}, 1600 cm^{-1} and 1270 cm^{-1} peaks with the base of the intensity at 20°C. Note that several phase transitions are clearly recognized.

which has been assigned to the twisted biphenyl vibrational mode, abruptly increases at the transition temperature to $S^*_{C_A}$ and increases continuously. This fact suggests that the benzene rings in the biphenyl group start to experience a flip-flop thermal motion [14] when the phase transition takes place to the $S^*_{C_A}$ phase. This kind of motion seems to affect the vibration of the C–C stretching of the biphenyl link (1285 cm^{-1}). Actually the intensity of the 1285 cm^{-1} peak relative to that of the 1270 cm^{-1} peak, which also shows the typical temperature dependence illustrated in figure 5, increases remarkably as shown in figure 6 (*b*) and figure 2 (*a*).

3.2. *DSC measurements*

In the Raman scattering experiments mentioned in the previous section, we showed that two different crystalline structures are formed depending on the cooling rate. The crystallization process was also observed by DSC. Figure 7 shows DSC curves obtained at different cooling rates. There are two exothermic peaks below 100°C. A small peak at 66°C corresponds to the transition from the $S^*_{C_A}$ phase to the $S^*_{I_A}$ phase [3]. A large peak is observed around 30°C on cooling faster than -2°C min^{-1}, as reported by Chandani *et al.* [3]. But this peak, which is attributed to the $S^*_{I_A}$–Cryst I

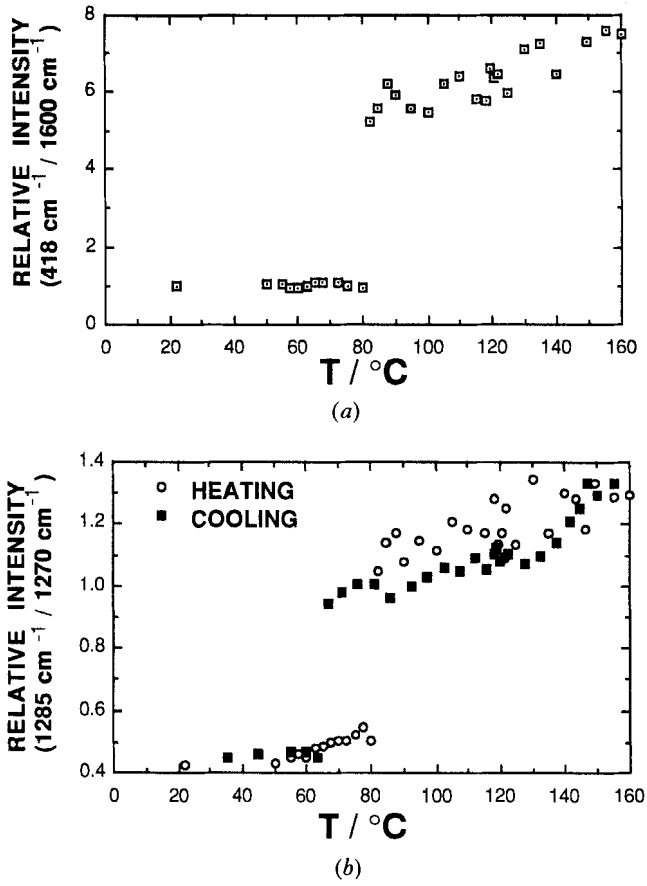

Figure 6. The exceptional temperature dependence of (*a*) the 418 cm^{-1} peak intensity relative to the 1600 cm^{-1} intensity and (*b*) the 1285 cm^{-1} peak intensity relative to the 1270 cm^{-1} intensity.

phase transition, dramatically shifts to higher temperature with decreasing cooling rate. At a cooling rate of $-1{\cdot}5°C\,min^{-1}$, another peak appears at a higher temperature and is attributed to the $S^*_{I_A}$–Cryst III phase transition. Thus, the DSC profile at a cooling rate of $-1{\cdot}5°C\,min^{-1}$ raises the possibility that two kinds of crystals coexist at room temperature when crystallization occurs under this condition. At a cooling rate of $-1°C\,min^{-1}$, only one peak is observed; this shifts toward the higher temperature side with decreasing cooling rate, and finally overlaps with the small peak corresponding to the transition from $S^*_{C_A}$ to $S^*_{I_A}$. Therefore, it is difficult to characterize the $S^*_{I_A}$ phase of MHPOBC, because crystallization occurs easily in the monotropic $S^*_{I_A}$ phase, and critically depends on cooling rate, holding time, impurities etc.

The enthalpy changes on crystallization are almost the same for rates higher than $-2°C\,min^{-1}$ ($\Delta H \sim -21\,kJ\,mol^{-1}$). However, the enthalpy discontinuously increases at a cooling speed of $-1{\cdot}5°C\,min^{-1}$ and reaches a saturated value ($\Delta H \sim -27{\cdot}1\,kJ\,mol^{-1}$) as the cooling rate becomes slower.

The thermal behaviour on the heating process is very complicated. Figure 8 shows DSC curves obtained at different heating rates. According to the experimental result of Raman scattering, when Cryst I is heated, transition to Cryst III occurs before the

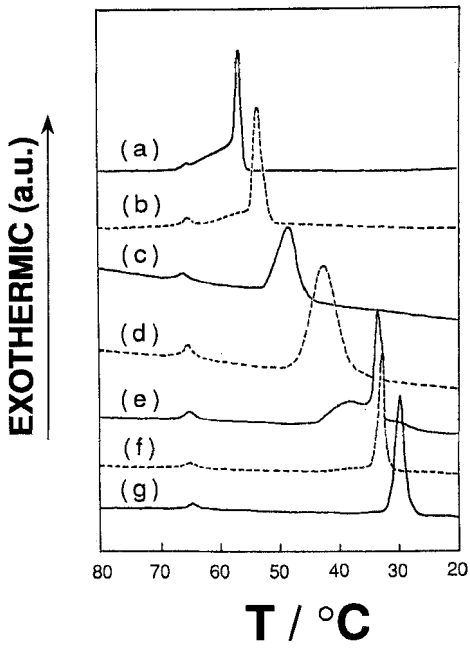

Figure 7. DSC thermogram at various cooling rates. The enthalpy change on crystallization is: (*a*) $\Delta H = -27{\cdot}12\,\text{kJ mol}^{-1}$ ($-0{\cdot}1\,^{\circ}\text{C min}^{-1}$), (*b*) $\Delta H = -27{\cdot}00\,\text{kJ mol}^{-1}$ ($-0{\cdot}25\,^{\circ}\text{C min}^{-1}$), (*c*) $\Delta H = -26{\cdot}79\,\text{kJ mol}^{-1}$ ($-0{\cdot}5\,^{\circ}\text{C min}^{-1}$), (*d*) $\Delta H = -25{\cdot}88\,\text{kJ mol}^{-1}$ ($-1\,^{\circ}\text{C min}^{-1}$), (*e*) $\Delta H = -25{\cdot}44\,\text{kJ mol}^{-1}$ ($-1{\cdot}5\,^{\circ}\text{C min}^{-1}$), (*f*) $\Delta H = -21{\cdot}20\,\text{kJ mol}^{-1}$ ($-2{\cdot}0\,^{\circ}\text{C min}^{-1}$) and (*g*) $\Delta H = -20{\cdot}81\,\text{kJ mol}^{-1}$ ($-5{\cdot}0\,^{\circ}\text{C min}^{-1}$).

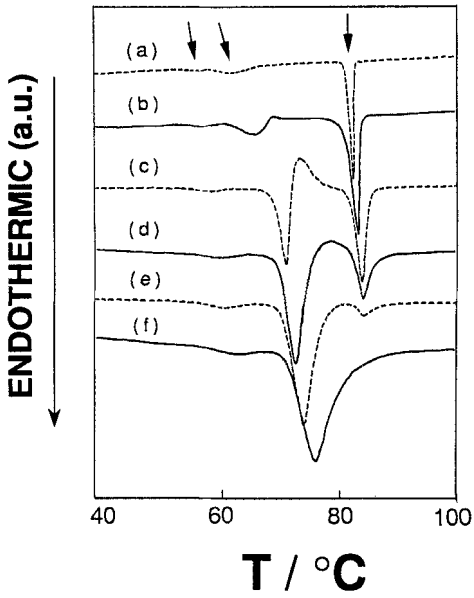

Figure 8. DSC thermograms starting from Cryst I at different heating rates; (*a*) $0{\cdot}5\,^{\circ}\text{C min}^{-1}$, (*b*) $1\,^{\circ}\text{C min}^{-1}$, (*c*) $3\,^{\circ}\text{C min}^{-1}$, (*d*) $7\,^{\circ}\text{C min}^{-1}$, (*e*) $10\,^{\circ}\text{C min}^{-1}$ and (*f*) $20\,^{\circ}\text{C min}^{-1}$. The arrows indicate three endothermic peak positions.

transition to the $S^*_{C_A}$ phase, as shown in figure 3 (*a*). Actually, however, Cryst I transformed to another crystalline phase, which is designated as Cryst II, before the transition to Cryst III [15]. In the DSC curves at heating rates slower than 10°C min^{-1}, three endothermic peaks are observed as indicated by the arrows in figure 8. The two peaks on the lower temperature side shift toward higher temperature with increasing heating rate, while the remaining peak stays at about 84°C. The lowest small peak is assigned to the Cryst I–Cryst II phase transition. We should notice that one exothermic peak is observed between two large endothermic peaks at 1, 3 and 7°C min^{-1}. Therefore, the middle endothermic and exothermic peaks are attributed to partial melting and recrystallization to Cryst III, respectively. It is clear that the highest temperature peak originates from the Cryst III–$S^*_{C_A}$ phase transition. A full discussion will be given in § 4.1.

3.3. *X-ray diffraction*

X-ray diffraction experiments were performed to determine the layer thickness. Let us first show the overall temperature variation of the layer thickness in figure 9. The layer thickness decreases when the temperature decreases from the S_A phase because of the tilt of molecules in the $S^*_{C_\alpha}$, S^*_C, $S^*_{C_\gamma}$ and $S^*_{C_A}$ phases. However, it begins to increase at about 90°C, and surprisingly exceeds that of the S_A in the $S^*_{I_A}$ phase region around 60°C. Then, the layer thickness discontinuously splits into larger and smaller values depending on the modes of crystallization.

In order to see the crystallization condition more clearly, the diffraction patterns were measured after controlled cooling. Figures 10 (*a*) and (*b*) show X-ray diffraction profiles under two different conditions of fast (-2°C min^{-1}) and slow ($-0{\cdot}7$°C min^{-1}) cooling, respectively. Fast cooling produces only one crystalline phase, whose long periodicity is about 32 Å; this phase is obtained from the $S^*_{I_A}$ phase with a layer thickness of about 35·7 Å at 50°C, as shown in figure 10 (*a*). From the Raman experiments, the crystal formed by fast cooling is Cryst I. Thus, only Cryst I which has a periodicity of 32 Å exists after fast cooling.

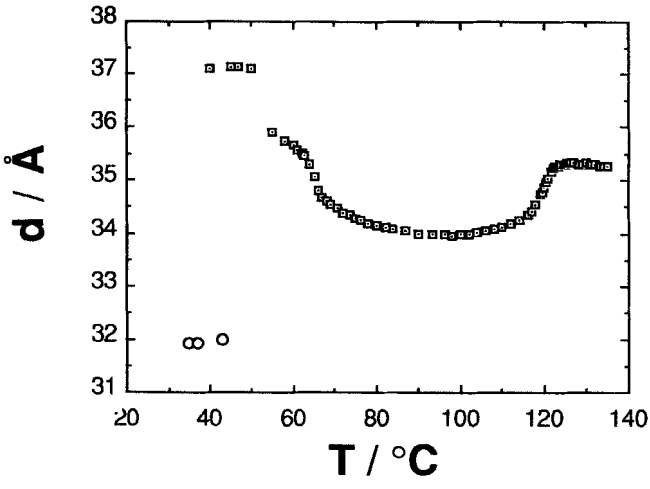

Figure 9. The overall temperature dependence of layer thickness in MHPOBC.

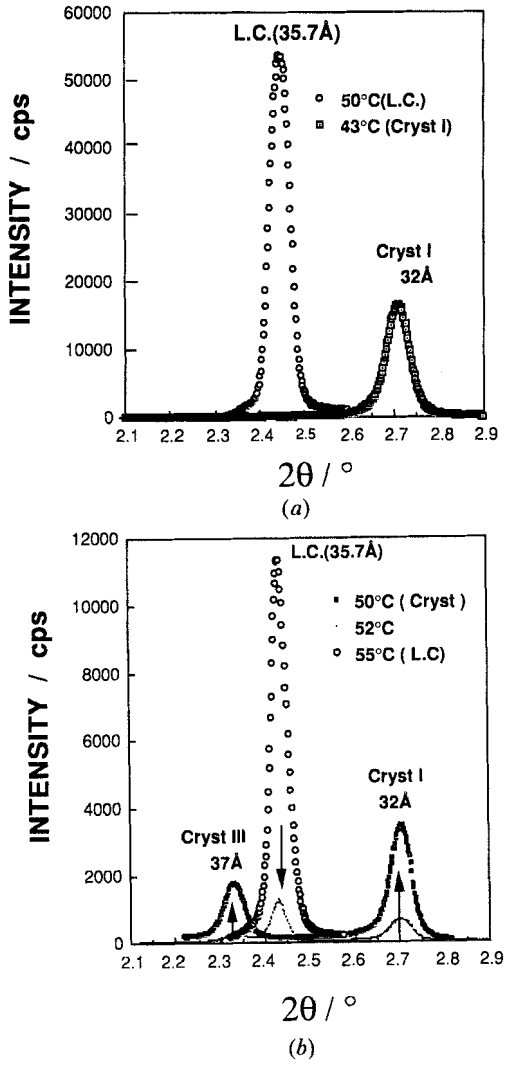

Figure 10. X-ray diffraction profiles at several temperatures when cooled at rates of (*a*) $-2°C\,min^{-1}$ and (*b*) $-0{\cdot}7°C\,min^{-1}$.

For a slowly cooled sample, however, there exist two peaks at diffraction angles corresponding to periodicities of 32 Å and 37 Å. These results confirm that the two different crystals, Cryst I and Cryst III, can coexist at room temperature and indicate that Cryst III has a periodicity of 37 Å.

Table 3 summarizes the proportions of Cryst III, calculated from powder X-ray diffraction peak areas, obtained at various cooling rates. The critical cooling rate at which Cryst III begins to be formed is slightly different from that determined by DSC because the crystallization modes depend on several factors. In any event, Cryst III is not obtained at a cooling rate higher than $-2°C\,min^{-1}$ and its fraction increases on slowing the rate. But pure Cryst III could not be obtained even at a cooling rate of $-0{\cdot}1°C\,min^{-1}$. Moreover, the presence of impurities appears to inhibit the formation of Cryst III. Pure Cryst III was obtained by annealing Cryst I at 74°C for 2 hours and subsequent slow cooling.

Table 3. Proportions of Cryst III calculated from the area ratio of powder X-ray diffraction peaks obtained at controlled cooling rates.

Cooling rate/°C min^{-1}	Per cent
−1·5	0·0
−1·0	0·0
−0·9	1·2
−0·8	34·4
−0·7	62·9
−0·5	69·2
−0·25	82·0
−0·1	96·3

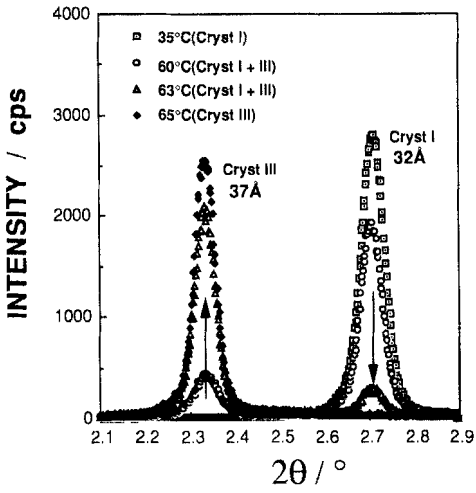

Figure 11. The variation of X-ray diffraction profiles on heating from Cryst I.

To increase knowledge about the crystal–crystal phase transition, X-ray diffraction profiles were observed by heating a sample of the Cryst I phase, as shown in figure 11. The diffraction peak at 32 Å corresponding to Cryst I decreases with increasing temperature. On the contrary, the X-ray diffraction peak of 37 Å becomes larger at the expense of the 32 Å peak and finally the latter peak disappears at 65°C.

4. Discussion

4.1. *Thermodynamic characteristics*

In the previous sections, we have described experimental results of Raman scattering, DSC and X-ray diffraction and shown that there exist two crystalline phases at room temperature, whose proportion critically depends on the cooling rate. Let us discuss the thermodynamic behaviour in this temperature range. Figure 12 shows the DSC thermogram for Cryst I and Cryst III on a heating process together with the schematic diagram of the Gibb's free energy concerning the phase transitions. As already shown in figure 8, three endothermic peaks (1, 2 and 4) are located around 58°C, 70°C and 84°C and one exothermic peak (3) at 73°C is observed for Cryst I when heated at 3°C min^{-1}, while the thermodynamically more stable Cryst III exhibits only one

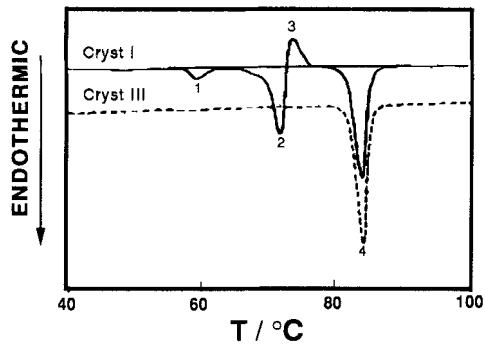

(*a*)

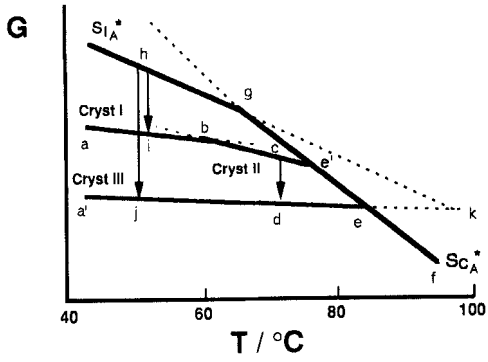

(*b*)

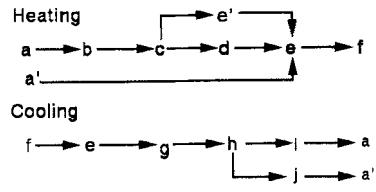

(*c*)

Figure 12. Phase transitions of MHPOBC; (*a*) DSC curves at a heating rate of 3°C min^{-1} from Cryst I and Cryst III, (*b*) schematic diagram of the Gibb's free energy where the arrow indicates spontaneous stabilization, and (*c*) all the possible phase sequences for heating and cooling processes.

endothermic peak at 84°C. The structure of Cryst I was studied in detail by X-ray diffraction and was assigned to the monoclinic structure [15]. Therefore peak 1 is ascribed to the transition from this monoclinic Cryst I to Cryst II with a different structure, although the structure is not known at this moment. This is the process shown in b in figure 12 (*b*).

The peak 2 seems to correspond to partial melting during the process b→c in figure 12 (*b*). We suspect that the alkyl chains start to melt on heating in the Cryst II phase. This kind of structural disturbance induces recrystallization to the most stable Cryst III, during which a conformational change from the largely bent structure to an extended one occurs, as will be discussed in detail in § 4.2. This process is observed as an

exothermic peak 3 in figure 12 (*a*) and corresponds to the process c→d. Hence, the partial melting and the Cryst II–Cryst III transition start to occur immediately after the temperature is raised over the point b. In this respect, it is hard to observe any particular phenomena in the Cryst II phase, since this phase always exists together with Cryst III. Actually the Raman peak around 1190 cm^{-1} shows no other particular state than Cryst I and Cryst III in the heating process, as shown in figure 3 (*a*).

According to Hori and Endo [15], the endothermic peak 2 was assigned to the Cryst II–$S^*_{C_A}$ phase transition at the point e′ in figure 12 (*b*) and hence the exothermic peak 3 was attributed to the recrystallization process from $S^*_{C_A}$ to Cryst III, i.e. during the process e′→e. Our assignments mentioned above are different from theirs. The occurrence of the process through b→c→d in figure 12 (*b*) is supported by the Raman spectra. As shown in figure 13, the strong low frequency Raman peaks at about 48 cm^{-1}, 75 cm^{-1} and 95 cm^{-1} resulting from lattice vibration only slightly lose their intensities above 70°C and then disappear above 85°C. This result indicates that at least one crystalline phase almost remains around and below 85°C which corresponds to the Cryst III–$S^*_{C_A}$ transition temperature. Therefore the intermediate state around the temperature of endothermic peak 2 in figure 12 (*a*) has more crystalline than liquid crystalline characteristics. Considering these facts, it is reasonable to conclude that the endothermic peak 2 corresponds to partial melting of alkyl chains and that recrystallization to Cryst III (peak 3 in figure 12 (*a*)) occurs before the transition to $S^*_{C_A}$. These assignments are also confirmed from the experimental results that, in the temperature range between 66°C and 84°C, we could not find any trace of conformational change in the biphenyl and carbonyl groups, which obviously occurs at the crystal–smectic phase transition as shown in figure 4 and figure 6, and as will be discussed in detail in § 4.3.

As shown in figure 8, the Cryst I–Cryst II transition temperature, as well as the partial melting and recrystallization temperatures, depend on the heating rate. On slow heating, the enthalpy change due to partial melting and recrystallization becomes smaller spuriously, since they occur simultaneously. When heated at a higher rate,

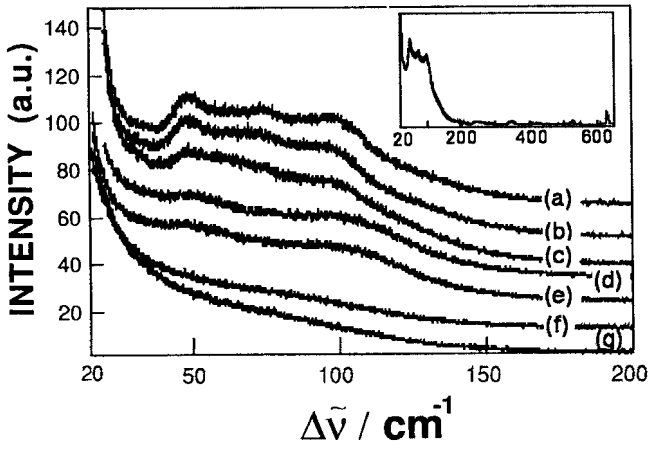

Figure 13. The temperature dependence of the low frequency Raman peaks; (*a*) 25°C, (*b*) 50°C, (*c*) 60°C, (*d*) 70°C, (*e*) 78°C, (*f*) 85°C and (*g*) 150°C. Inset is to show the intensities of these low frequency peaks as compared with the higher ones such as 630 cm^{-1}.

however, it seems that Cryst II directly changes to $S^*_{C_A}$ in a similar way to tripalmitin [16] and 2-amino-4-(*N*-methylanilino)-6-isopropenyl-s-triazine [17]. This is the process via e′ in figure 12 (*b*).

On the other hand, the Cryst III–$S^*_{C_A}$ transition occurs at 84°C on heating while the $S^*_{C_A}$ phase expands its temperature range to 66°C in the cooling process, where the phase transition to $S^*_{I_A}$ occurs irrespective of the cooling rate as shown in figure 7. Therefore, the $S^*_{C_A}$ phase in the temperature range from 66°C to 84°C, i.e. region g–e in figure 12 (*b*), is metastable like the region a–b, b–c–e′ and g–h. To confirm this, the stability of a homogeneously aligned cell at 74°C was observed through an optical microscope. The alignment was maintained during 24 hours, but was thoroughly broken as expected after 26 hours.

MHPOBC crystallizes from $S^*_{I_A}$ to Cryst I (h→i) or to Cryst III (h→j) depending on cooling speed, as shown in figure 10. The dependence is influenced by holding time, impurity, etc. Cryst I can be transformed to Cryst III by heating or annealing, but the latter cannot metamorphose into the former without passing through liquid crystalline phases. In this respect, Cryst I is a monotropic phase. The reasons why metastable Cryst I is more easily formed than stable Cryst III may be that the crystallization rate to Cryst I is faster than that to Cryst III and that the difference in Gibb's free energy is relatively small. All the possible phase sequences are schematically depicted in figure 12 (*c*).

4.2. *Structures of the two crystalline phases*

Now let us consider the structural differences between Cryst I and Cryst III. Recently Hori and Endo [15] clarified the structure of Cryst I by X-ray analysis. According to their report, monoclinic Cryst I has a smectic-like layer structure composed of largely bent molecules; the alkyl chain with the chiral group is attached almost perpendicularly (93°) to the core part and is highly disordered with a twisted conformation, while the normal paraffin chain is relatively extended. The torsional angle of the benzene–benzene linkage in the biphenyl group is 4·3°. Although the structure of Cryst I has been disclosed as mentioned above, there is no report on Cryst III. We will consider the structure of Cryst III qualitatively by comparing the differences in several spectra. The structural differences are summarized as follows.

(1) The biphenyl moiety is almost coplanar and the torsional angle is less than 4·3° for Cryst III. This inference can be drawn from the following experimental facts. (*a*) Figure 14 shows the temperature dependence of Raman spectrum in the frequency range between 390 cm^{-1} and 450 cm^{-1}. The 418 cm^{-1} peak in Raman spectrum was recently assigned to a vibrational mode of a twisted biphenyl group by Tashiro *et al.* [14]. Although the 408 cm^{-1} and 428 cm^{-1} peaks which locate near the 418 cm^{-1} make the spectra complicated, the temperature dependence of the 418 cm^{-1} peak is clearly observed. This peak almost disappears in Cryst III (72°C), while a small peak still exists in Cryst I (25°C). This peak intensity becomes larger as the temperature approaches the Cryst III–$S^*_{C_A}$ transition temperature. The disappearance of this peak in Cryst III suggests a planar structure. (*b*) The in-plane C–H deformation vibration of the benzene ring at 1190 cm^{-1} shifts to 1198 cm^{-1} for Cryst III, as shown in figure 3. This is due to the increase in steric interactions between the 2,2′-hydrogen atoms with decrease in the dihedral angle between the two benzene rings [13]. (*c*) Recently Sone *et al.* [18], found in ^{13}C NMR spectrum that the chemical shift of carbon e (see figure 1), 142 ppm, gradually shifts upfield as the dihedral angle of biphenyl decreases. We found that chemical shift of carbon e moves upfield by 0·6 ppm in Cryst III.

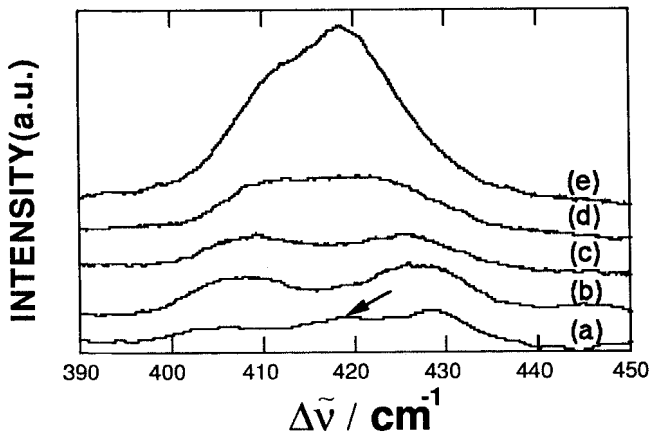

Figure 14. The temperature dependence of the Raman spectrum in the frequency range of 390–450 cm^{-1}; (*a*) 25°C, (*b*) 72°C, (*c*) 80°C, (*d*) 83°C and (*e*) 85°C.

(2) When the phase transition takes place from Cryst I to Cryst III, the Raman shift of C=O stretching at k_1 in figure 1 (between biphenyl and phenyl groups) moves to a lower frequency by 2·2 cm^{-1} in Cryst III, while that at k_2 (appended to the chiral group) shifts to higher frequency by 3·6 cm^{-1}, as shown in the inset of figure 2 (*a*). This means that the k_1 C=O bonding strength is weaker and that for k_2 is stronger in Cryst III than in Cryst I. The vibrational energy can be affected by intermolecular and intramolecular interactions and molecular conformations. In the present case, the conformational contribution must be important because of the following reasons: (*a*) There are no functional groups inducing a strong intermolecular interaction such as hydrogen bonding and (*b*) the intermolecular distance of about 4 Å [15] for MHPOBC is too large for significant interaction by considering Kuhn's results [19] which contend that a hydrogen bond is difficult to form when the O···H distance is larger than 3·3 Å. Therefore, these vibrational energy differences may result from the dihedral angles of the two carbonyl groups with respect to the neighbouring benzene rings. The benzene ring donates electrons toward the carbonyl group, and hence the bonding strength becomes weak, as the carbonyl group increases in coplanarity with the benzene ring and thus is resonance-stabilized [8, 20]. Further studies are required for a more detailed discussion.

(3) In the ^{13}C CP/MAS NMR spectra for Cryst I and Cryst III, there are serious changes in the carbons 6, 8, 9, 10 and 11 (see figure 1) which are located close to the rigid mesogenic core. This supports the existence of the conformational difference between Cryst I and Cryst III especially at the boundary of mesogenic core and flexible alkyl chain. As clearly shown by the X-ray experiments (see figure 10), Cryst III has a longer periodicity than Cryst I by 5 Å, so that Cryst III is thought to involve a relatively extended conformation, contrary to the largely bent conformation at the chiral group for Cryst I. The details for the Cryst III structure are now being studied by ^{13}C solid state NMR.

4.3. *Structure in the liquid crystalline phases*

The result of the C=O stretching shown in figure 4 implies a structural change at the crystal–S^*_{CA} phase transition. In the crystalline phases, the carbonyl groups tend to be planar with the benzene rings, although the degree of coplanarity may differ according

to the crystal forms or the positions at which the carbonyls are attached. However, departures from coplanarity do occur in the liquid crystalline phases and cause the frequencies of the C=O stretching to increase due to the weakening in resonance-stabilization (see figure 4 (*a*)). The carbonyls may be rotated out of the planes of their corresponding benzene rings with a certain distribution. The distribution of the rotation angle, probably the dynamic one, would tend to broaden the C=O stretching peaks, as shown in figure 4 (*c*) and figure 1 (*a*), since each state contributes to its own stretching frequency. A similar conformational discussion has already been reported based on Raman spectra for polyethyleneterephthalate [20].

Another piece of structural information associated with the crystal–$S^*_{C_A}$ phase transition is supplied by the temperature variation of the 418 cm^{-1} peak. As mentioned in § 3.1, the biphenyl group starts to experience a benzene ring flip-flop vibration at the Cryst III–$S^*_{C_A}$ phase transition. The motion is reflected in the jump observed in figure 6 (*a*). The increase in the intensity with increasing temperature implies gradual growth of the flip-flop motion. This implication can also be confirmed by the chemical shift of carbon e in figure 1 obtained by the ^{13}C CP/MAS NMR spectrum; 142·8 ppm at 25°C (Cryst I), 142·2 ppm at 70°C (Cryst III), 145·57 ppm at 130°C (S_A), 146·06 ppm at 160°C (I) and 146·25 ppm in $CDCl_3$ solution. The details will be reported in a separate paper.

5. Conclusions

Raman scattering, DSC measurements and X-ray diffraction experiments were made on MHPOBC. We found that two crystalline phases are formed depending on cooling rates, and that these two kinds of crystal can coexist at room temperature when crystallized under proper conditions. Discussion has been given for the thermodynamic characteristics around the crystal–$S^*_{C_A}$ phase transition region based on DSC measurements. The conformational changes have been discussed based on Raman spectra and X-ray diffraction: Dihedral angles between the benzene rings and the carbonyl groups and between the two benzene rings of the biphenyl group characteristically change at the crystal–$S^*_{C_A}$ phase transition. The carbonyl groups rotate around the C–C bond connecting the benzene ring and the carbonyl group, and the biphenyl group experiences a flip-flop twisting vibration in the liquid crystalline phases.

The authors thank Mr M. Sone and Professor J. Watanabe of the Department of Polymer Chemistry in TIT for measuring the ^{13}C NMR spectrum and their valuable discussions. They also acknowledge Prof. K. Hori for discussing the X-ray analysis. This work was partly supported by a Grant-in-Aid for Scientific Research (#03205045) from the Ministry of Education, Science and Culture and by the Casio Science Promotion Foundation.

References

[1] CHANDANI, A. D. L., HAGIWARA, T., SUZUKI, Y., OUCHI, Y., TAKEZOE, H., and FUKUDA, A., 1988, *Jap. J. appl. Phys.*, **27,** L729.

[2] CHANDANI, A. D. L., GORECKA, E., OUCHI, Y., TAKEZOE, H., and FUKUDA, A., 1989, *Jap. J. appl. Phys.*, **28,** L1265.

[3] CHANDANI, A. D. L., OUCHI, Y., TAKEZOE, H., FUKUDA, A., TERASHIMA, K., FURUKAWA, K., and KISHI, A., 1989, *Jap. J. appl. Phys.*, **28,** L1261.

[4] YAMADA, Y., YAMAMOTO, N., MORI, K., NAKAMURA, K., HAGIWARA, T., SUZUKI, Y., KAWAMURA, I., ORIHARA, H., and ISHIBASHI, Y., 1990, *Jap. J. appl. Phys.*, **29,** 1757.

[5] BULKIN, B. J., 1972, *Advances in Infrared and Raman Spectroscopy*, Vol. 8, edited by R. J. H. Clark and R. E. Hester (Heyden & Son), Chap. 3.

[6] AMER, N. M., and SHEN, Y. R., 1972, *J. chem. Phys.*, **56,** 15.

[7] IKEDA, A., TAKANISHI, Y., TAKEZOE, H., and FUKUDA, A., 1993, *Jap. J. appl. Phys.*, **32,** L97.
[8] GEORGE, W. O., and MCINTYRE, P. S., 1987, *Infrared Spectroscopy*, edited by D. J. Mowthorpe (John Wiley & Sons), Chap. 7.
[9] COLTHUP, N. B., DALY, L. H., and WIBERLEY, S. E., 1975, *Introduction to Infrared and Raman Spectroscopy* (Academic Press), Chaps. 8 and 9.
[10] VERGOTEN, G., and FLEURY, G., 1976, *J. molec. Struct.*, **30,** 347.
[11] KOZIELSKI, M., BAUMAN, D., DROZDOWSKI, M., and SALAMON, Z., 1987, *Molec. Crystals liq. Crystals*, **142,** 1.
[12] GRAY, G. W., and MOSLEY, A., 1976, *Molec. Crystals liq. Crystals*, **35,** 71.
[13] TAKASE, A., SAKAGAMI, S., and NAKAMIZO, M., 1978, *Jap. J. appl. Phys.*, **17,** 1495.
[14] TASHIRO, K., HOU, J. A., KOBAYASHI, M., and INOUE, T., 1990, *J. Am. chem. Soc.*, **112,** 8273.
[15] HORI, K., and ENDO, K., 1993, *Bull. chem. Soc. Japan*, **66,** 46.
[16] KUNIHISA, K. S., 1973, *Bull. chem. Soc. Japan*, **46,** 2862.
[17] YUKI, Y., TAIKA, T., and NAGANO, M., 1972, *Bull. chem. Soc. Japan*, **45,** 3494.
[18] SONE, M., and WATANABE, J. (private communication).
[19] KUHN, L. P., 1952, *J. Am. chem. Soc.*, **74,** 2492.
[20] MELVEGER, A. J., 1972, *J. Polym. Sci. Phys. Ed.*, **10,** 317.